Mechanical Systems and Signal Processing 49 (2014) 118–134

Contents lists available at ScienceDirect

Mechanical Systems and Signal Processing

journal homepage: www.elsevier.com/locate/ymssp

An investigation of the dynamic electromechanical coupling effects in machine drive systems driven by asynchronous motors

Tomasz Szolc*, Robert Konowrocki, Maciej Michajłow, Agnieszka Pręgowska

Institute of Fundamental Technological Research of the Polish Academy of Sciences, ul. A. Pawińskiego 5B, 02-106 Warsaw, Poland

ARTICLE INFO

Article history:
Received 31 May 2013
Received in revised form
1 April 2014
Accepted 5 April 2014
Available online 15 May 2014

Keywords:
Machine drive system
Asynchronous motor
Electromechanical coupling

ABSTRACT

In the paper dynamic electromechanical interaction between the rotating machine drive system and the electric driving motor is considered. The investigations are performed by means of the circuit model of the asynchronous motor as well as using an advanced structural hybrid model of the drive system. Using the analytical solutions applied for the electrical and the mechanical systems the electromagnetic stiffness and coefficient of damping, both generated by the electric motor rotationally interacting with the mechanical system of the given dynamic properties, were determined. By means of experimentally validated computational responses obtained for torsional harmonic excitation induced by the driven machine working tool, a modification of dynamic properties of the mechanical system by the electromagnetic flux between the stator and the rotor has been studied.

1. Introduction

Torsional vibrations of drive systems usually result in a significant fluctuation of the rotational speed of the rotor of the driving electric motor. Such oscillations of the angular speed superimposed on the average rotor rotational speed cause more or less severe perturbation of the electromagnetic flux and thus additional oscillations of the electric currents in the motor windings. Then, the generated electromagnetic torque is also characterized by additional variable in time components which induce torsional vibrations of the drive system. According to the above, mechanical vibrations of the drive system become coupled with the electrical vibrations of currents in the motor windings. Such a coupling is often complicated in character and thus computationally troublesome. Because of this reason, till now majority of authors simplify the matter regarding mechanical vibrations of drive systems and electric current vibrations in the motor windings as mutually uncoupled. Then, the mechanical engineers applied the electromagnetic torques generated by the electric motors as '*a priori*' assumed excitation functions of time or the rotor-to-stator slip, e.g. in [1–3], usually based on numerous experimental measurements carried out for the given electric motor dynamic behaviors. For this purpose, by means of measurement results, proper approximate formulas have been developed, which describe respective electromagnetic external excitations produced by the electric motor [2]. However, the electricians thoroughly modeled electric current flows

* Corresponding author. Tel.: +48 22 8261281x319; fax: +48 22 8269815.
E-mail address: tszolc@ippt.pan.pl (T. Szolc).

http://dx.doi.org/10.1016/j.ymssp.2014.04.004
0888-3270/

in the electric motor windings, but they usually reduced the mechanical drive system to one or seldom to at most a few rotating rigid bodies, as e.g. in [4]. In many cases, such simplifications yield sufficiently useful results for engineering applications, but very often they can lead to remarkable inaccuracies, since many qualitative dynamic properties of the mechanical systems, e.g. their mass distribution, torsional flexibility and damping effects, are being neglected. Thus, an influence of drive system vibratory behavior on the electric machine rotor angular speed fluctuation, and in this way on the electric current oscillations in the rotor and stator windings, cannot be investigated with a satisfactory precision.

Currently fast development of machinery driven by electric motors is observed which requires bigger and bigger knowledge about dynamic interaction between the mechanical and electrical parts of the entire system. An importance of the electromechanical coupling effects taken into consideration is particularly significant when possibly exact results are required for investigation of extremely responsible drive systems or for analyses of their sufficiently precise and stable motions as well as in order to elaborate proper active vibration control algorithms. This problem has been already studied for many years and by many authors, but in majority of cases sufficiently accurate electromechanical models are not usually used, e.g. because of the above mentioned far-reaching simplifications of the mechanical system. For example, in [5] an influence of '*a priori*' assumed rotor angular speed oscillation on the electromagnetic torque fluctuations was investigated by means of the circuit model of the asynchronous motors. In [6] rotor-shaft transient torsional vibrations in the turbogenerator sets caused by network disturbances were considered as coupled with the electric current vibrations in the generator windings. Coupling effects between the geared drive system torsional vibrations and the electric current oscillations in the synchronous motor windings were investigated in [7], where the current flows in the electric machine windings were modeled using Park's equations. In the case of synchronous machines the complex torque coefficients method is commonly applied in order to determine the torsional vibration frequency dependent electromagnetic stiffness and damping coefficient, where negative value zones of the latter indicate a probability of dynamic instabilities. Advantages and drawbacks of this approach are described in [8]. A practical application of the complex torque coefficients method has been demonstrated in [9] for the coupled electromechanical vibration analysis of the multi-generator drive system. In [10,11] the dynamic interaction between the asynchronous or synchronous motors and the drive system was studied, where the motor electromagnetic flux was modeled using two-dimensional finite elements and the drive train was substituted by means of the simple spring-mass model. In these papers the above mentioned electromagnetic stiffness and damping coefficient have also been determined for the synchronous and various asynchronous motors, where the torsional perturbations were excited by the use of '*a priori*' assumed test impulses of the motor rotor angular speed.

Nowadays, a severity of the electromechanical interaction is commonly observed in the case of so called 'variable speed drives' (VSD) of large rotating machines driven by synchronous or asynchronous motors controlled by the load commutated inverters. In transient and steady-state operating conditions these devices are responsible for generating additional fluctuating driving torque components which can be a source of unexpected dangerous resonance effects of torsional vibrations. Some results of theoretical and experimental investigations in this field have been reported e.g. in [12,13]. Coupled electromechanical interactions were also studied in [14] using the circuit model of the stepping motor driving a precise mechanism modeled by means of the advanced hybrid torsional train consisting of torsionally deformable continuous structural macro-elements and discrete dynamic oscillators.

As it follows from numerous observations, drive systems of several machines driven by the asynchronous motors commonly indicate diverse sensitivity to resonance effects following from their mechanical eigenvibration properties. It is suspected that for almost complete attenuation of resonance effects at resonant frequencies of excitation induced by the driven machine retarding torque as well as for unexpected severe amplification of torsional vibration amplitudes forced by a non-resonant excitation the above mentioned additional torsional elasticity and viscosity introduced into the mechanical system by the electromagnetic flux generated in the electric motor are responsible. In order to explain such dynamic behavior better, in this paper a qualitative analysis of the electromechanical coupling effects for several rotating machine drive systems driven by various asynchronous motors during their steady-state operation are performed. The investigations are carried out by means of the circuit model of the electric motor and using the advanced structural hybrid model of the rotating machine drive system. Some theoretical results have been confirmed by measurements performed on the real objects.

2. Modeling of the mechanical system

In order to investigate a character of the electromechanical coupling, the possibly realistic and reliable mechanical model of the drive system is applied. In this paper, similarly as e.g. in [14–16], dynamic investigations of the entire drive system are performed by means of the one-dimensional hybrid structural model consisting of finite continuous visco-elastic macro-elements and rigid bodies. In this model by the torsionally deformable cylindrical macro-elements of continuously distributed inertial-visco-elastic properties the successive cylindrical segments of the stepped shafts and coupling disks are substituted, as shown in Fig. 1. In order to obtain a sufficiently accurate representation of the real object, the visco-elastic macro-elements in the hybrid model are characterized by the geometric cross-sectional polar moments of inertia J_{Ei} responsible for their elastic and inertial properties as well as by the separate layers of the polar moments of inertia J_{Ii} responsible for their inertial properties only, $i=1, 2, \ldots, n$, where n is the total number of macro-elements in the considered hybrid model. The inertias of gear-wheels and driven machine working tools are represented by rigid bodies attached to the appropriate macro-element cross-sections.

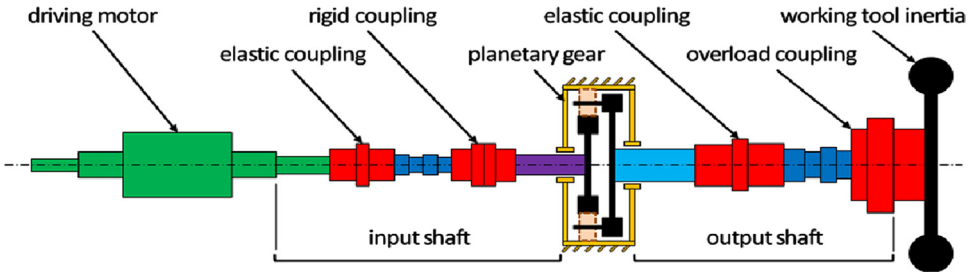

Fig. 1. Hybrid mechanical model of the drive system.

Torsional motion of cross-sections of each visco-elastic macro-element is governed by the hyperbolic partial differential equations of the wave type

$$G_i J_{Ei}\left(1+\tau\frac{\partial}{\partial t}\right)\frac{\partial^2\theta_i(x,t)}{\partial x^2}-c_i\frac{\partial\,\theta_i(x,t)}{\partial t}-\rho(J_{Ei}+J_{Ii})\frac{\partial^2\theta_i(x,t)}{\partial t^2}=q_i(x,t), \tag{1}$$

where $\theta_i(x,t)$ is the angular displacement with respect to the shaft rotation with the average angular speed Ω, τ denotes the retardation time in the Voigt model of material damping, G_i is the Kirchhoff (shear) modulus of the model i-th macro-element material and c_i denotes the coefficient of external (absolute) damping. In the considered case, this kind of damping is caused by retarding torques due to friction forces in the bearings and aerodynamic forces. The active and the passive external torques are continuously distributed along the respective macro-elements of lengths l_i. These torques are described by the two-argument functions $q_i(x,t)$, where x is the spatial co-ordinate and t denotes the time.

Mutual connections of the successive macro-elements creating the stepped shaft as well as their interactions with the rigid bodies are described by equations of boundary conditions. These equations contain geometrical conditions of compliance for rotational displacements of the extreme cross sections for $x=L_i=l_1+l_2+\ldots+l_{i-1}$ of the adjacent $(i-1)$-th and the i-th elastic macro-elements

$$\theta_{i-1}(x,t)=\theta_i(x,t)\quad \text{for } x=L_i. \tag{2a}$$

The second group of boundary conditions are dynamic ones, which contain linear equations of equilibrium for external torques as well as for inertial, elastic and external damping moments. For example, the dynamic boundary condition describing a simple connection of the mentioned adjacent $(i-1)$-th and the i-th elastic macro-elements has the following form:

$$M_i(t)-I_{0i}\frac{\partial^2\theta_i}{\partial t^2}-G_{i-1}J_{E,i-1}\left(1+\tau\frac{\partial}{\partial t}\right)\frac{\partial\theta_{i-1}}{\partial x}+G_iJ_{Ei}\left(1+\tau\frac{\partial}{\partial t}\right)\frac{\partial\theta_i}{\partial x}=0 \quad \text{for} \quad x=L_i,\quad i=2,3,\ldots,n, \tag{2b}$$

where $M_i(t)$ denotes the external concentrated torque and I_{0i} is the mass polar moment of inertia of the rigid body.

In order to perform an analysis of natural elastic vibrations, all the forcing and viscous terms in the motion Eq. (1) and boundary conditions (2b) have been omitted. An application of the solution of variable separation for Eq. (1) leads to the following characteristic equation for the considered eigenvalue problem:

$$\mathbf{C}(\omega)\times\mathbf{D}=\mathbf{0}, \tag{3}$$

where $\mathbf{C}(\omega)$ is the real characteristic matrix and $\mathbf{D}$ denotes the vector of unknown constant coefficients in the analytical local eigenfuctions of each i-th macro-element, as derived e.g. in [15]. Thus, the determination of natural frequencies reduces to the search for values of ω, for which the characteristic determinant of matrix $\mathbf{C}$ is equal to zero. Then, the torsional eigenmode functions are obtained by solving Eq. (3).

The solution for forced vibration analysis has been obtained using the analytical–computational approach described e.g. in [15,16]. Solving the differential eigenvalue problem (1)–(3) and an application of the Fourier solution in the form of series in the orthogonal eigenmode functions lead to the set of uncoupled modal equations for time coordinates $\xi_m(t)$

$$\ddot{\xi}_m(t)+(\beta+\tau\omega_m^2)\dot{\xi}(t)+\omega_m^2\xi(t)=\frac{1}{\gamma_m^2}\left(X_m^S\cdot T_{el}(t)-X_m^R\cdot M_r(t)\right),\quad m=1,2,\ldots \tag{4}$$

where ω_m are the successive natural frequencies of the drive system, β denotes the coefficient of external damping assumed here as proportional to the modal masses γ_m^2, $T_{el}(t)$ denotes the external torque generated by the electric motor, $M_r(t)$ is the driven machine retarding torque and X_m^S, X_m^R are the modal displacements scaled by proper maxima and corresponding to the electric motor- and to the driven machine working tool-locations in the hybrid model, respectively. A mathematically proven fast convergence of the applied Fourier solution enables us to reduce the number of the modal equations to solve in order to obtain a sufficient accuracy of results in the given range of frequency. Here, it is necessary to solve only 6–10 modal equations (4), even in cases of very complex mechanical systems, contrary to the classical finite element formulation leading usually to large numbers of motion equations corresponding each to more than 100 or many hundreds degrees of freedom, even in the case of one-dimensional beam element applications. Then, in order to minimize a numerical effort, the artificial

and often error-prone model reduction algorithms have to be applied as an additional task in the entire computational routines.

3. Modeling of the electric motor

From the viewpoint of electromechanical coupling investigation, in the introductory approach, the properly advanced circuit model of the electric motor seems to be sufficiently accurate. The symmetrical three-phase asynchronous motor electric current oscillations in its windings are described by the six circuit voltage equations transformed next into the system of four Park's equations in the so called '$\alpha\beta$–dq' reference system

$$\begin{bmatrix} \sqrt{\frac{3}{2}}U\cos(\omega_e t) \\ \sqrt{\frac{3}{2}}U\sin(\omega_e t) \\ 0 \\ 0 \end{bmatrix} = \begin{bmatrix} L_1+\frac{1}{2}M & 0 & \frac{3}{2}M & 0 \\ 0 & L_1+\frac{1}{2}M & 0 & \frac{3}{2}M \\ \frac{3}{2}M & 0 & L_2'+\frac{1}{2}M & 0 \\ 0 & \frac{3}{2}M & 0 & L_2'+\frac{1}{2}M \end{bmatrix} \cdot \begin{bmatrix} \dot{i}_\alpha^s(t) \\ \dot{i}_\beta^s(t) \\ \dot{i}_d^r(t) \\ \dot{i}_q^r(t) \end{bmatrix}$$

$$+ \begin{bmatrix} R_1 & 0 & 0 & 0 \\ 0 & R_1 & 0 & 0 \\ 0 & \frac{3}{2}pM\Omega(t) & R_2' & p\Omega(t)(L_2'+\frac{1}{2}M) \\ -\frac{3}{2}pM\Omega(t) & 0 & -p\Omega(t)(L_2'+\frac{1}{2}M) & R_2' \end{bmatrix} \cdot \begin{bmatrix} i_\alpha^s(t) \\ i_\beta^s(t) \\ i_d^r(t) \\ i_q^r(t) \end{bmatrix}, \tag{5}$$

where U denotes the power supply voltage, ω_e is the supply voltage circular frequency, L_1, L'_2 are the stator coil inductance and the equivalent rotor coil inductance, respectively, M denotes the relative rotor-to-stator coil inductance, R_1, R'_2 are the stator coil resistance and the equivalent rotor coil resistance, respectively, p is the number of pairs of the motor magnetic poles, $\Omega(t)$ is the current rotor angular speed including the average and vibratory components and i_α^s, i_β^s are the electric currents in the stator windings reduced to the electric field equivalent axes α and β and i_d^r, i_q^r are the electric currents in the rotor windings reduced to the electric field equivalent axes d and q, [17]. Then, the electromagnetic torque generated by such a motor can be expressed by the following formula:

$$T_{el} = \frac{3}{2}pM(i_\beta^s i_d^r - i_\alpha^s i_q^r). \tag{6}$$

4. Solution of the problem

From the form of Park's equations (5) as well as from formula (6) it follows that the coupling between the electric and the mechanical systems is non-linear in character, particularly for significantly varying motor rotational speeds $\Omega(t)$. Such a coupling leads to very complicated analytical description resulting in rather harmful computer implementation. Thus, this electromechanical coupling can be realized here by means of the step-by-step numerical extrapolation technique, which for relatively small direct integration steps for Eqs. (4) and (5) results in very effective, stable and reliable results of computer simulation.

Nevertheless, for steady-state operating conditions with the constant average motor rotational speed Ω_n, i.e. for $\Omega(t)=\Omega_n+\Theta(t)$, where $|\Theta(t)|\ll\Omega_n$, in order to obtain more qualitative information about the character of electromechanical coupling in the drive system, based on the harmonic balance method, an approximate analytical solution for currents in Park's equations has been applied in the following form:

$$i_\mu^\nu = (\Phi_\mu^\nu + A_\mu^\nu(t))\sin(\omega_e t) + (\Psi_\mu^\nu + B_\mu^\nu(t))\cos(\omega_e t), \tag{7}$$

where $A_\mu^\nu(t)$, $B_\mu^\nu(t)$ are the unknown time-functions to be determined, $\mu=\alpha$, β for $\nu=s$ and $\mu=d$, q for $\nu=r$. The symbols Φ_μ^ν, Ψ_μ^ν denote the constants, for which (7) satisfies Park's equations (5) for $A_\mu^\nu(t)$, $B_\mu^\nu(t)=0$ and for $\Omega(t)=\Omega_n=$const. It is to emphasize here that for such Φ_μ^ν, Ψ_μ^ν, by substituting (7) for $A_\mu^\nu(t)$, $B_\mu^\nu(t)=0$ into (6), using the well known trigonometric identities and upon neglecting small terms of higher order, values of the static component of the electromagnetic motor torque for various constant rotational speeds Ω_n are obtained. By means of these torque-to-speed relationships the asynchronous motor static torque characteristics are determined.

For the assumed sinusoidal external excitation generated by the driven machine $M_r(t)=R\sin(\omega t)$, the fluctuating component of the motor rotational speed $\Omega(t)$ is expected also in the harmonic form: $\Theta(t)=G\sin(\omega t)+H\cos(\omega t)$, where $|G|$, $|H|\ll\Omega_n$. Then, for the already determined constants Φ_μ^ν, Ψ_μ^ν one can assume:

$$A_\mu^\nu(t) = C_\mu^\nu sin(\omega t) + D_\mu^\nu cos(\omega t) \text{ and } B_\mu^\nu(t) = E_\mu^\nu sin(\omega t) + F_\mu^\nu cos(\omega t), \tag{8}$$

where $\mu=\alpha$, β for $\nu=s$ and $\mu=d$, q for $\nu=r$. Next, by substituting (8) into (7), and (7) into Park's equations (5) and upon proper grouping of the terms standing respectively in front of the sine and cosine functions and then upon evaluating the

determined in this way sums to zero, the following system of 16×16 linear algebraic equations is obtained:

$$\mathbf{C}(\Omega_n,\omega_e,\omega)\cdot\mathbf{D}=\mathbf{E}(\mathbf{B},G,H), \tag{9}$$

where $\mathbf{C}$ denotes the matrix of circuit resistances and inductances, $\mathbf{B}=\mathrm{col}(\ldots\Phi^{\nu}_{\mu}\ldots,\ldots\Psi^{\nu}_{\mu}\ldots)$, $\mathbf{D}=\mathrm{col}(\ldots C^{\nu}_{\mu}\ldots,\ldots D^{\nu}_{\mu}\ldots,\ldots E^{\nu}_{\mu}\ldots,\ldots F^{\nu}_{\mu}\ldots,)$ and $\mathbf{E}$ is the input vector of the sine- and cosine-amplitudes of the fluctuating component of the motor rotational speed $\Theta(t)$. By solving (9), substituting the elements of vector $\mathbf{D}$ first into (7) and then into (6) and upon neglecting small terms of higher order, the sine- and cosine-amplitudes of the fluctuating component of the motor torque are obtained in the following form:

$$T^{\mathrm{var}}_{el}(t)=S(\omega)\sin(\omega t)+T(\omega)\cos(\omega t), \tag{10}$$

where

$$S(\omega)=\tfrac{3}{2}pM(\Psi^s_\beta E^r_d+\Psi^r_d E^s_\beta-\Psi^s_\alpha E^r_q-\Psi^r_q E^s_\alpha)$$
$$T(\omega)=\tfrac{3}{2}pM(\Psi^s_\beta F^r_d+\Psi^r_d F^s_\beta-\Psi^s_\alpha F^r_q-\Psi^r_q F^s_\alpha).$$

In this way, the fluctuating component of the electromagnetic torque induced by the drive system torsional oscillations has been separated from the average torque value. For the above mentioned harmonic retarding torque generated by the driven machine and for the harmonic electromagnetic motor torque external excitations obtained in (10) a solution of modal equations (4) becomes also harmonic. Then, by means of the well known analytical solutions of such ordinary differential equations and using the mode superposition solution, dynamic responses of the considered mechanical system can be determined. For example, the sine- and cosine-amplitudes G and H of the fluctuating component of the motor rotational speed $\Theta(t)$ are obtained in the following form:

$$G=-\omega\cdot W,\ W=\sum_{m=0}^{\infty}\frac{(X^S_m)^2T(\omega)\cdot(\omega^2_m-\omega^2)-[(X^S_m)^2S(\omega)-X^S_mX^R_mR]\cdot(\beta+\tau\omega^2_m)\omega}{\gamma^2_m[(\omega^2_m-\omega^2)^2+(\beta+\tau\omega^2_m)^2\omega^2]},$$
$$\text{and } H=\omega\cdot U,\ U=\sum_{m=0}^{\infty}\frac{[(X^S_m)^2S(\omega)-X^S_mX^R_mR]\cdot(\omega^2_m-\omega^2)+(X^S_m)^2T(\omega)\cdot(\beta+\tau\omega^2_m)\omega}{\gamma^2_m[(\omega^2_m-\omega^2)^2+(\beta+\tau\omega^2_m)^2\omega^2]}. \tag{11}$$

Then, by expressing S and T as in (10), substituting them into (11) and by inserting (11) into (9), upon proper rearrangements one obtains the following system of 16×16 linear algebraic equations describing electromechanical coupling effects in the drive system:

$$\mathbf{C}(\Omega_n,\omega_e,\omega,\omega_m,\gamma^2_m,\beta,\tau)\cdot\mathbf{D}=\mathbf{F}(\omega_m,\gamma^2_m,\beta,\tau,\omega,R). \tag{12}$$

Here, matrix $\mathbf{C}$ as well as input vector $\mathbf{F}$ became functions of the mechanical system dynamic parameters. It is to notice that the system of algebraic Eq. (12) is linear with respect to the retarding torque amplitude R. Solutions of (12) for various retarding torque fluctuation frequencies ω and amplitudes R enable us to determine the sine- and cosine-amplitudes of the oscillating component of the asynchronous motor torque using (10). By projecting the sine- and cosine-components of the electromagnetic torque and of the rotor rotation angle respectively on the complex plane real and imaginary axes and using the proper definitions given e.g. in [11], the electromagnetic torsional stiffness $k_e(\omega)$ and the coefficient of damping $d_e(\omega)$ generated by the asynchronous motor are determined in the following form:

$$k_e(\omega)=-\frac{U\cdot S(\omega)+W\cdot T(\omega)}{U^2+W^2},\quad d_e(\omega)=-\frac{1}{\omega}\cdot\frac{U\cdot T(\omega)-W\cdot S(\omega)}{U^2+W^2}, \tag{13}$$

where the sine- and cosine-angular displacement amplitudes U and W have been already defined in (11). The above expressions (7)–(13) derived by means of the proposed analytical–computational approach enable us to determine dynamic characteristics of the coupled electromechanical system. It is to remark that up till now the electromagnetic stiffness and damping coefficient of the electric motors were usually determined as functions of '*a priori*' assumed rotor angular speed amplitudes corresponding to given excitation frequencies, as e.g. in [5] or [11]. In this way, these quantities are independent of the mechanical system dynamic properties. But here, the rotor angular speed amplitudes G and H are expressed in the form of mechanical system amplitude frequency characteristics (11) and thus the electromagnetic stiffness and damping coefficient (13) became also functions of the drive system dynamic properties. These functions will be presented in the following examples.

5. Computational and experimental examples

The above derived analytical solution for the electromechanical model will be illustrated by means of three examples of various rotating machine drive systems driven by diverse asynchronous motors. Fundamental parameters of these motors are provided in Table 1. In all cases the considerations are going to be focused on the interaction frequency ranges containing the fundamental, first torsional eigenfrequencies. These systems will be studied in steady-state operating conditions under sinusoidal external excitation generated by the driven machine with the assumed test amplitudes R in the range between 0.15 and 0.50 of the nominal torque, which is quite common for crushers, mills, pulverizers, drilling devices, pumps and others. First, the drive system start-ups into steady-state operation are going to be numerically simulated by the

Table 1
Fundamental parameters of the asynchronous motors.

Nominal power [kW]	22	932	2.1
Nominal rotational speed [rpm]	1465	892	1680
Rated torque [Nm]	143	9977.5	12
Supplied voltage [V]	400	4000	390
Voltage frequency [Hz]	50	60	60

use of modal equations (4), Park's equations (5) and expression (6). Then, the qualitative analyses will be carried out using the analytical–computational approach expressed by relations (10)–(13). Moreover, in two cases the theoretical findings will be compared with analogous results of measurements performed on the real objects.

5.1. *Example I: coal pulverizer geared drive system*

In the first example the drive system of the small power industrial coal pulverizer equipped with proper measurement devices is considered, as shown in Fig. 2. This machine is driven by the 22 kW asynchronous motor by means of the reduction planetary gear of the resultant ratio 1:5.33 as well as by the use of the spur gear of the ratio 1:31 reducing a rotational speed of the pulverizer drum. The static torque characteristic of this motor, determined using relationships (5)–(7), is shown in Fig. 3a. The drive system is equipped with two torque-meters installed respectively in the input shaft, i.e. between the electric motor and the gear stage, and in the output shaft, i.e. between the gear stage and the coal pulverizer. Since the torsional flexibility of the entire pulverizer drum is incomparably smaller than the torsional flexibilities of the all drive system components, its huge mass moment of inertial has been reduced to the output-shaft axis and substituted in the mechanical model by means of the rigid body attached to the end of this shaft.

The hybrid model of this drive system has been properly tuned-up in order to be characterized by the corresponding fundamental torsional natural frequencies possibly close to these obtained experimentally. For this purpose the mechanical system with the turned-off driving motor was induced to torsional vibrations by means of the hydraulic shaker. The sinusoidal external signal generated by this device within the frequency range 0–50 Hz was successively imposed to various points of the tested object in order to determine three fundamental torsional natural frequencies by the use of

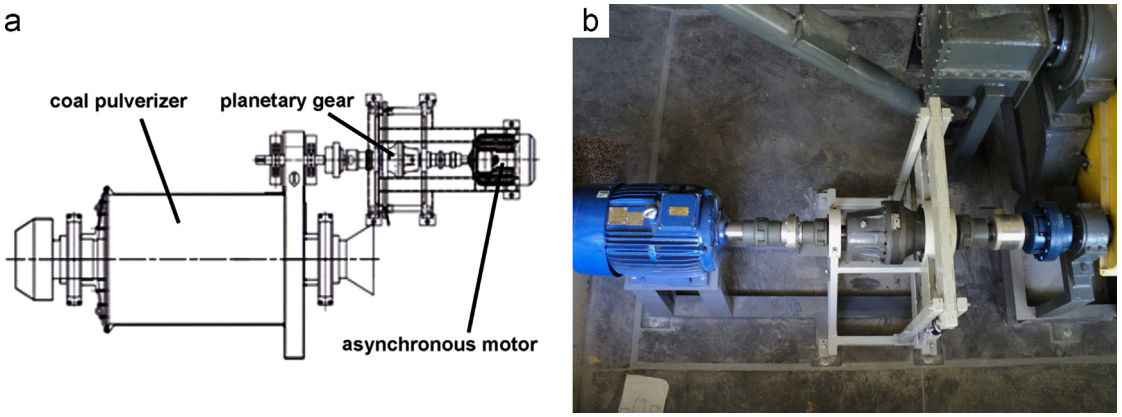

Fig. 2. Coal pulverizer drive system: the scheme (a) and the real object with the measurement equipment (b).

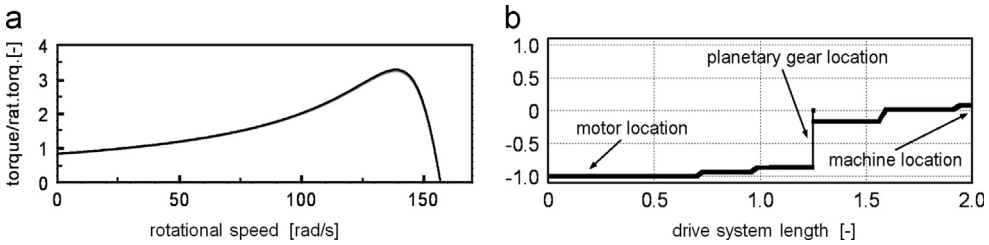

Fig. 3. Static torque characteristic of the driving motor (a) and the first eigenform of the drive system (b).

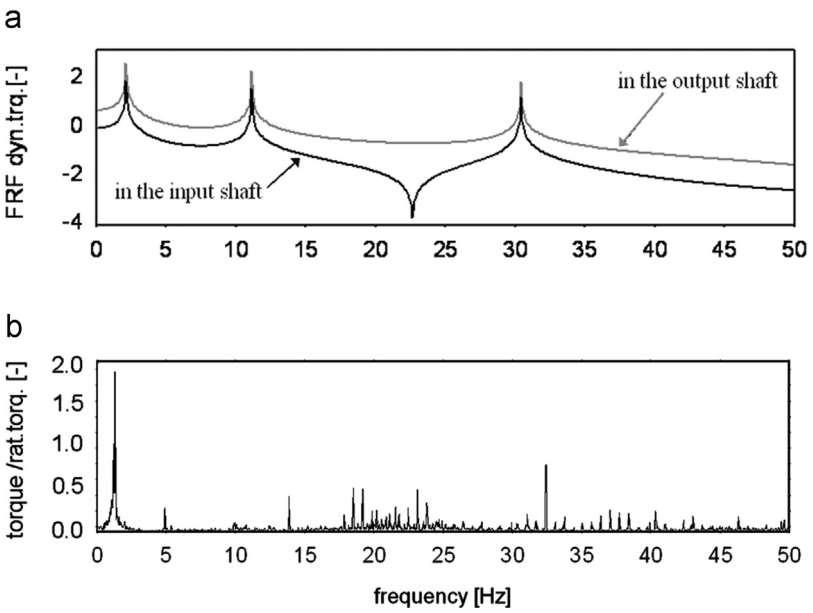

Fig. 4. Calculated frequency response function of the mechanical system (a) and amplitude characteristic of the measured dynamic torque transmitted by the system input shaft (b).

measurements of the vibration amplitudes and signal-to-response phase angles. Apart from the rigid body mode of zero frequency, naturally existing for rotating systems, the measured values of the first three 'elastic' natural frequencies are equal to 2.1, 14.7 and 33.4 Hz. Despite a relatively complex structure of the real pulverizer drive system, characterized by many parameters difficult to identify, the proper tuning of selected theoretical constants resulted in a quite good agreement of the natural torsional vibration behavior between the hybrid mechanical model and the real object. Namely, the first three calculated 'elastic' natural frequency values are equal to 2.1, 11.6 and 30.8 Hz. The first torsional eigenform of frequency 2.1 Hz, computationally obtained using the identified hybrid mechanical model, is depicted in Fig. 3b. In Fig. 4a, the theoretically determined frequency response functions of this system, regarded as purely mechanical are shown. Their plots are characterized by the significant peaks corresponding approximately to the above mentioned first three torsional natural frequencies.

Simultaneously, in this model the mechanical damping level was identified. For this purpose the tuned-up hybrid model was harmonically excited to forced, steady-state torsional vibrations within the above mentioned frequency range 0–50 Hz in an analogous way as the real object by means of the hydraulic shaker. In order to adjust the computational vibration amplitudes respectively to these registered using measurements, the damping coefficient β and the retardation time τ in the modal equations (4) have been properly selected to obtain mutual relative differences not exceeding 3% for resonant conditions, where damping usually plays a particularly significant role. By the use of this approach the mechanical eigenvibration properties and damping level have been determined to establish a background for further dynamic investigations with the turned-on driving motor generating the electromagnetic stiffness and electromagnetic damping.

Then, the real coal pulverizer drive system was experimentally tested in nominal, steady-state operating conditions for the supply voltage frequency set-up to $\omega_e/2\pi=50$ Hz, where on the rated torque the fluctuating sinusoidal component of amplitude $R=0.15$ of the constant value has been imposed by the hydraulic shaker within the excitation frequency range $\omega/2\pi=0$–50 Hz, regarded as practically the most important. Here, in the case of rotating system the hydraulic shaker was attached to the planetary gear housing flexibly suspended in the solid immovable frame which is visible in Fig. 2. In this way, it was possible to introduce into the pulverizer drive system loading the harmonically fluctuating component, the amplitude of which has been selected using the shaker performances as well as the geometrical dimensions and the gear ratios of the planetary gear.

In Fig. 4b, the amplitude spectrum determined by means of FFT of the measured dynamic torque time histories and registered using the torque-meter installed in the system input-shaft, i.e. between the driving motor and the gear stage is presented, see Fig. 2. Apart from the peak observed at $\sim$5 Hz and of the peaks occurring in the vicinity of the anti-resonance, i.e. within 18–25 Hz, see Fig. 4a, which can be interpreted as disturbances introduced by unexpected external excitations, one can notice the significant peaks corresponding to ca. 14 and 32.5 Hz. These peaks are related to resonance effects with the system's second and the third natural frequencies. Moreover, the first, predominant peak of frequency $\sim$1.53 Hz seems apparently to indicate a resonance effect with the system fundamental, first 'elastic' eigenform. But from the analogous amplitude spectra determined for the real system steady-state operating conditions for the supply voltage frequencies set-up to $\omega_e/2\pi=40$, 30, 20, 10 and 5 Hz it followed that these predominant peaks were corresponding to the excitation frequencies $\omega/2\pi\cong 1.20$, 0.533, 0.44, 0.133 and 0.067 Hz, while the frequency values related to the significant

peaks resulting from resonance effects with the second and the third natural frequencies remained unchanged, i.e. they differed not more than ± 0.15 Hz. For the above listed supply voltage frequencies the average rotational speed values of the input and output shafts were appropriately proportional to these supply frequencies. Moreover, the supply voltages were properly selected to keep in each case the average torque values in the input and output shafts approximately the same as those for 50 Hz. The complete set of results of the measurements performed in this way is provided in Table 2. According to the above, these predominant, the most severe, low-frequency vibration amplitudes are not an effect of classical mechanical resonances, but they seem to be induced by the dynamic interaction with the driving asynchronous motor. In order to explain this phenomenon, the qualitative analysis of the considered electromechanical system has been carried out.

From results of the numerical simulation performed for the above mentioned resonant frequency $\omega/2\pi=2.1$ Hz of the retarding torque fluctuation it follows that completely no resonance effects are obtained, which indicate the plots in Fig. 5a and b. In Fig. 5a, the black and gray lines respectively demonstrate the time histories of the electromagnetic motor torque and of the driven machine retarding torque reduced to the motor axis. In Fig. 5b the respective time histories of dynamic torques transmitted by the input (black line) and output (gray line) shafts during start-up and steady-state operation are depicted. This comment follows from the direct amplitude comparisons of the corresponding time histories of the both external excitation torques with those of the response dynamic torques transmitted by the above mentioned shaft segments. Namely, if time-histories of external excitations overlay with analogous response time-histories, then any so called dynamic amplification is observed and such responses can be regarded as quasi-static. This interpretation will be further applied for variable in time severe external excitations caused by the electromechanical interaction between the electric motor and the driven mechanical system. Here, no dynamic amplifications are observed, even the response amplitudes are smaller than the respective ones characterizing the external excitations. Thus, one can conclude that for this excitation frequency $\omega/2\pi=2.1$ Hz any resonance effect does not occur. However, the maximal amplitudes of the system dynamic response have been obtained for the retarding torque fluctuation frequency 1.67 Hz, which indicate the analogous results in Fig. 5c and d presented respectively in an identical way as these in Fig. 5a and b. From the analogous as mentioned above direct comparisons of the corresponding external excitation and dynamic response amplitudes it follows that here also no dynamic amplification is observed, but the electromagnetic torque fluctuation amplitudes significantly increased, contrary to the case of previously considered excitation frequency $\omega/2\pi=2.1$ Hz. In the retarding torque fluctuation frequency domain ω in Fig. 6a the plots of steady-state dynamic response fluctuation amplitudes determined by successive numerical simulations performed for the analogous system nominal operating conditions as these realized during measurements, i.e. for the supply voltage frequency set-up to $\omega_e/2\pi=50$ Hz are shown. In this figure the black and gray lines, respectively, there are the plotted amplitudes of the motor-torque and of the dynamic torque transmitted by the input shaft in the vicinity of the torque-meter position in the real object. Both the curves are characterized by three peaks corresponding to the excitation frequencies $\omega/2\pi \cong 1.67$, 11.6 and 30.8 Hz. Similarly as in the plot in Fig. 4b, the theoretically

Table 2
Results of measurements performed for the coal pulverizer drive system.

Supply voltage frequency [Hz]	50	40	30	20	10	5
Average input shaft rotat. speed [rpm]	1482	1192	886	580	281	128
Average output shaft rotat. speed [rpm]	282	219	166	100	49	16
Average torque in the input shaft [Nm]	78	77	76	74	71	70
Average torque in the output shaft [Nm]	386	382	381	370	356	353
Excitation frequency of the first, predominant vibration peak [Hz]	1.53	1.20	0.533	0.44	0.133	0.067

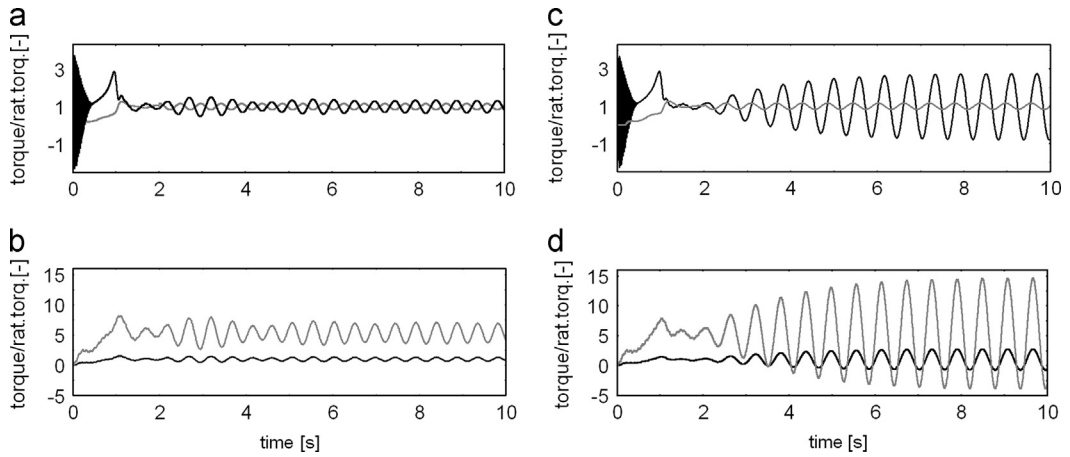

Fig. 5. Simulated dynamic response of the coal-pulverizer drive system: for the resonant mechanical frequency (a, b) and for maximal vibration amplitudes (c, d).

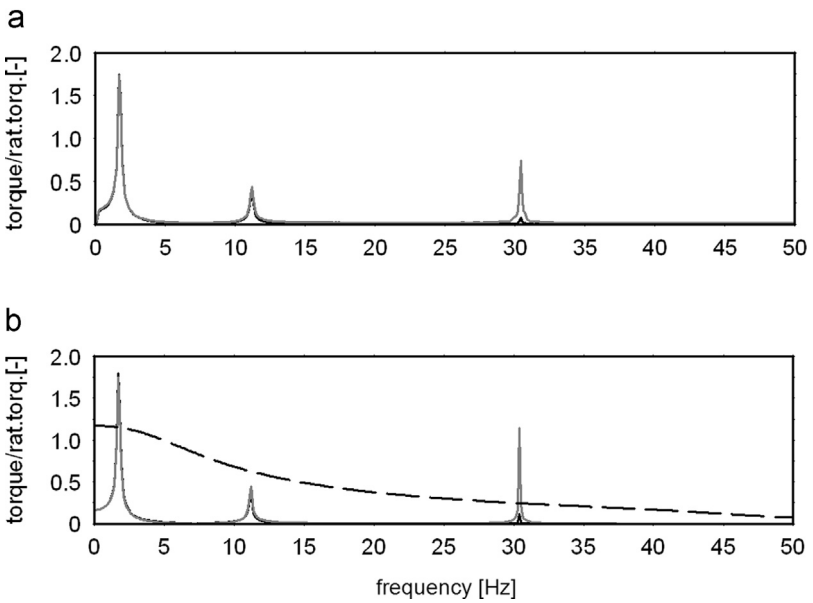

Fig. 6. Amplitude characteristics of the electromagnetic torque (solid black and dashed line) and of the mechanical torque in the input shaft (gray line) obtained using simulations (a) and by means of the analytical solution (b).

obtained second and the third peaks indicate resonance effects with the system torsional vibration respective eigenforms. The first, predominant peak of frequency 1.67 Hz corresponds to the above mentioned experimentally registered low-frequency vibration amplitudes. It is noted that in the case of this peak the amplitude of excitation generated by the driving motor is almost identical with the amplitude of the dynamic torque transmitted by the adjacent input-shaft. This fact substantiates a quasi-static character of these low-frequency oscillations, contrary to the above mentioned third, typical resonant peak, where a severe dynamic response amplification is observed. The result depicted in Fig. 6a and determined by successively repeated simulations performed each for constant excitation frequency values $\omega/2\pi$ within 0–50 Hz has been very precisely confirmed by the analogous plots in Fig. 6b obtained using the analytical relationships (10)–(12) and illustrated in the same way as in Fig. 6a. The electromagnetic torque amplitude characteristics depicted in Fig. 6a and b by means of the solid black lines have been determined as functions of the motor rotor angular speed fluctuation followed from the dynamic properties of the driven mechanical system excited to torsional vibrations with various frequencies ω in steady-state operating conditions. In Fig. 6b, for a comparison, using the black dashed line, an additional electromagnetic torque amplitude characteristic obtained for the arbitrarily assumed constant motor rotor angular speed fluctuation amplitude is presented, i.e. by means of solving Eq. (9) and using formula (10) for constant input sinusoidal and co-sinusoidal components G and H of the angular speed amplitude within the entire considered range of the excitation frequency ω. This characteristic demonstrates an asynchronous motor sensitivity to generation of the fluctuating component of the electromagnetic torque in the given range of rotor torsional vibration frequency. From this plot it follows that the greatest fluctuation of the driving torque is observed at the smallest rotor vibration frequencies, to decrease gradually with an increase of the frequency ω. This feature will be applied in the further explanation of the qualitative character of the electromechanical coupling between the asynchronous motor and the driven, torsionally vibrating mechanical system.

In addition, the analogous amplitude characteristics of the measured and theoretically obtained dynamic torque transmitted by the system output shaft, i.e. between the gear stage and the coal pulverizer, are presented in Fig. 7. In Fig. 7a the experimentally determined amplitude characteristic is shown. However, Fig. 7b presents two theoretically obtained amplitude characteristics, which almost mutually overlay each other, i.e. determined by the successive numerical simulations by means of modal equations (4), Park's equations (5) and expression (6) (gray line) as well as using the analytical formulae (10)–(12) (black line).

Moreover, in Fig. 8, also in the retarding torque fluctuation frequency domain ω, the black and gray lines, respectively, present the plots of electromagnetic stiffness and damping coefficient determined using formula (13). It is to emphasize that both curves in Fig. 8 are qualitatively similar to analogous electromagnetic stiffness and damping characteristics obtained in [11] by means of the above mentioned spatial flux model dynamically perturbed by the '*a priori*' applied rotor angular speed impulses assumed as entirely independent of the drive system properties and loadings. In order to estimate the mechanical system stiffening generated by the asynchronous motor, the electromagnetic stiffness values should be compared with mechanical model successive modal stiffness $\omega_i^2\gamma_i^2$, $i=1, 2,\ldots$, regarded here as approximate reference measures. For all torsional eigenfunctions normalized to unity the modal mass of the rigid body mode is equal to the entire mass moment of inertia of the considered drive system model, whereas the successive modal masses of the 'elastic' eigenmodes become respective fractions of this realistic value. Under this assumption the modal stiffness corresponding to successive torsional

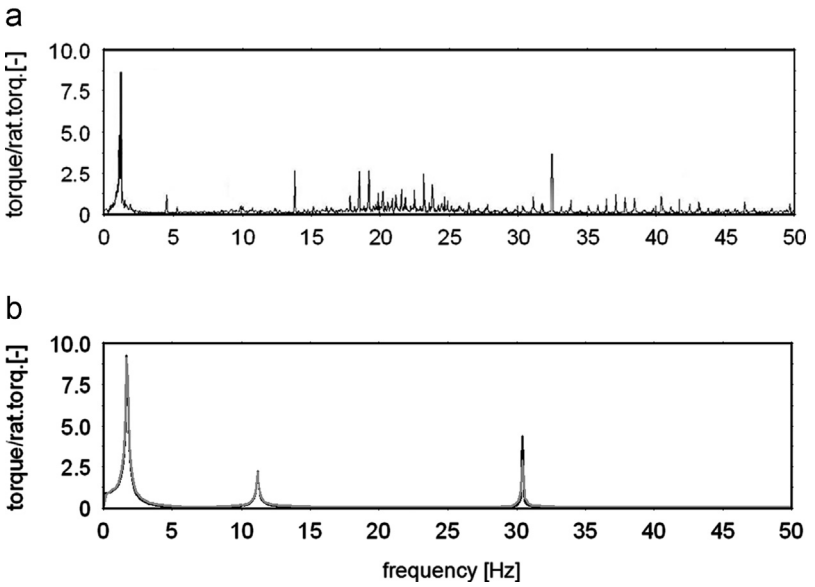

Fig. 7. Amplitude characteristics of the dynamic torque in the output shaft determined by means of measurements (a) and computations using simulations (gray line) and the analytical solution (black line) (b).

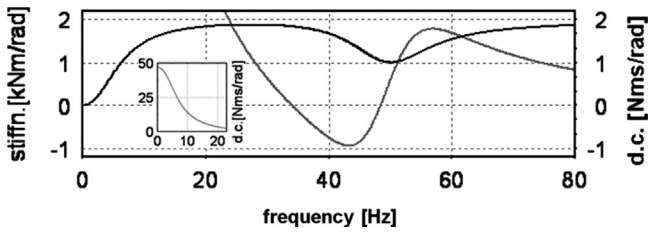

Fig. 8. Electromagnetic stiffness (black line) and damping coefficient (gray line).

natural frequencies can be compared with respective electromagnetic stiffness values determined by the characteristic shown in Fig. 8.

From the stiffness characteristic in Fig. 8 it follows that for the first system natural frequency 2.1 Hz the electromagnetic stiffness introduced by the asynchronous motor is equal to ca. 0.180 kNm/rad which exceeds the mechanical system first modal torsional stiffness $\omega_{1\gamma 1}^{2\,2}=0.169$ kNm/rad, to reach much greater values for higher interaction frequencies. Thus, the considered drive system is not a so called 'free–free' one, but it becomes visco-elastically clamped by the electromagnetic flux between the motor rotor and the stator. In general, this feature can significantly change system natural frequency values and corresponding to them torsional eigenforms. But in the considered case such electromagnetic visco-elastic spring has completely attenuated the resonance effect with the first eigenfrequency because of extremely high electromagnetic damping generated at low interaction frequencies, see Fig. 8. Moreover, it should be noted that the dynamic response amplification caused by the resonance effect with the second eigenform is very small, as a result of the very high electromagnetic damping in the range 0–20 Hz, see Figs. 6–8. In a contradistinction, as mentioned above, the dynamic response amplification caused by the resonance effect with the third eigenform becomes very severe, since the electromagnetic damping tends to zero for excitation frequencies $\omega/2\pi$ greater than 30 Hz. The natural frequency values of the second and the third 'elastic' eignenmodes have not been remarkably influenced by a stiffening caused by the electromagnetic spring. Namely, the second eigenform is characterized by the modal stiffness $\omega_{2\gamma 2}^{2\,2}=1.368$ kNm/rad comparable with the electromagnetic stiffness ca. 1.2 kNm/rad for $\omega/2\pi\cong 10.6$ Hz, see Fig. 8. But this eigenform is hardly excitable by the electric motor torque because of almost zero values of its eigenfuction at the motor location, contrary to e.g. the first 'elastic' eigenfunction shown in Fig. 3b. However, the third eigenform has the modal stiffness $\omega_{3\gamma 3}^{2\,2}=50.491$ kNm/rad which is much greater than the electromagnetic one, equal to ca. 1.9 kNm/rad for $\omega/2\pi\cong 30.8$ Hz, to be remarkably influenced. Moreover, it is to remember that according to the fundamentals of mechanical system vibration theory, eventually the slight increases of natural frequencies due to the electromagnetic stiffening effect become compensated by a common action of mechanical and electromagnetic damping. However, the maximum dynamic response at 1.67 Hz, without any dynamic amplification, is of a quasi-static character, induced by very high electric motor torque amplitudes occurring at low interaction frequencies. This fact follows from the above described additional motor-torque characteristic depicted by the dashed line in Fig. 6b and determined using relationships (9) and (10) for the arbitrarily assumed constant rotor angular speed

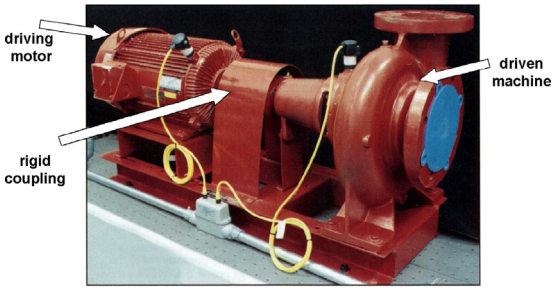

Fig. 9. The centrifugal blower driven by the asynchronous motor.

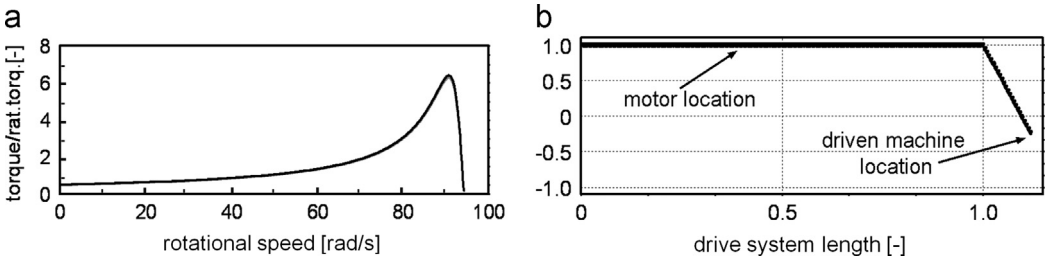

Fig. 10. Static torque characteristic of the driving motor (a) and the first eigenform of the drive system (b).

fluctuation amplitudes G and H within the entire considered frequency domain. Such electromechanical low-frequency dynamic behavior is also interpreted in the literature as rotational vibrations of the mechanical system rigid body mode, zero natural frequency of which is being increased by the stiffening caused by the electromagnetic spring generated by the driving motor.

It is also to emphasize that the plot of the electromagnetic damping shown in Fig. 8 indicates a negative damping zone in the range between 35 and 50 Hz, which for very small drive system mechanical damping can lead to operational instabilities. But in the considered case the experimentally identified level of shaft material and external damping protects the entire electromechanical system against instabilities and severe resonance effects.

The investigated, measurement available coal-pulverizer drive system with three elastic couplings is characterized by the above mentioned small first torsional 'elastic' natural frequency 2.1 Hz. It turned out that in this particular case the quantitative influence of the asynchronous motor interaction on the system low-frequency dynamic response seems to be negligible from the practical engineering viewpoint. Actually, the difference between the fundamental torsional 'elastic' resonant frequency and the excitation frequency ω corresponding to the predominant dynamic response low-frequency peak reaches only ca. 0.5 Hz. But it is to emphasize that, as described above in detail, the reason of these low-frequency oscillations is qualitatively of a completely different character than a typical ordinary 'elastic' resonance usually expected in a purely mechanical system. Nevertheless, the phenomenon investigated here of the drive system–asynchronous motor dynamic interaction should be additionally demonstrated by means of the more spectacular computational example described below.

5.2. *Example II: centrifugal blower drive system*

The character of electromechanical interaction studied above can be confirmed in the following example of the industrial centrifugal blower driven by the 932 kW asynchronous motor. In order to illustrate a structure of the considered machine, in Fig. 9 a smaller unit belonging to its entire type-series is presented. The static torque characteristic of this motor, determined in an identical way as that in the above example, is shown in Fig. 10a.

The first torsional 'elastic' eigenform of natural frequency 24.7 Hz of the considered drive system hybrid model is presented in Fig. 10b. Similarly as in the previous case, harmonic excitation caused by the retarding torque of the mentioned resonant frequency does not result in any remarkable response amplification in the steady-state operating conditions, which follows from that demonstrated in Fig. 11a and b simulation results of the system start-up into the nominal operation. However, the most severe electromechanical response is observed at the retarding torque fluctuation frequency 6.4 Hz, as shown in Fig. 11c and d in an identical way as in Fig. 5. Here, upon the passage through the transient resonance effects during run-up, the drive system becomes significantly affected by the low-frequency torsional oscillations. This fact has been confirmed by the analogous results of qualitative analysis presented in Fig. 12. Nevertheless, in this case, contrary to the previous example, the resonance effect with the first, fundamental torsional eigenmode has not been entirely suppressed, but 'shifted' into higher frequency 29.2 Hz, which follows from the comparison of the corresponding frequency response function of this mechanical system shown in Fig. 12a with the corresponding dynamic response amplitude characteristics obtained using numerical simulations and the proposed analytical–computational approach. The plots of

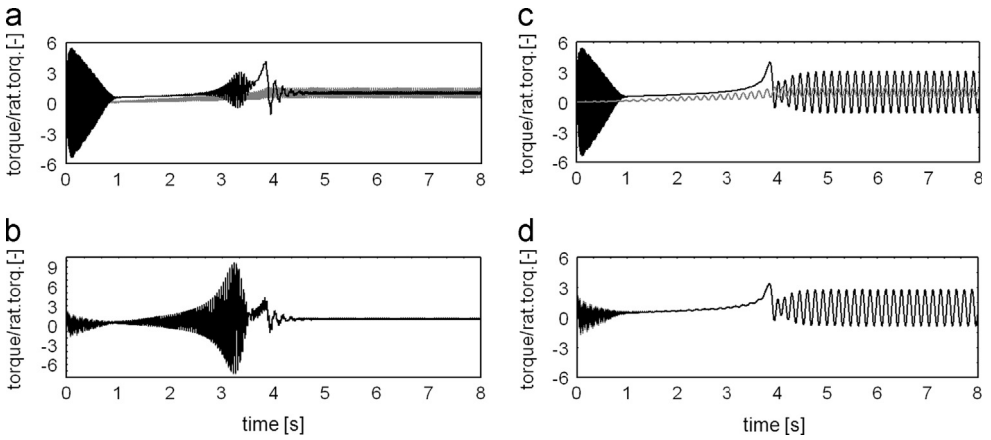

Fig. 11. Simulated dynamic response of the centrifugal blower drive system: for the resonant mechanical frequency (a, b) and for maximal vibration amplitudes (c, d).

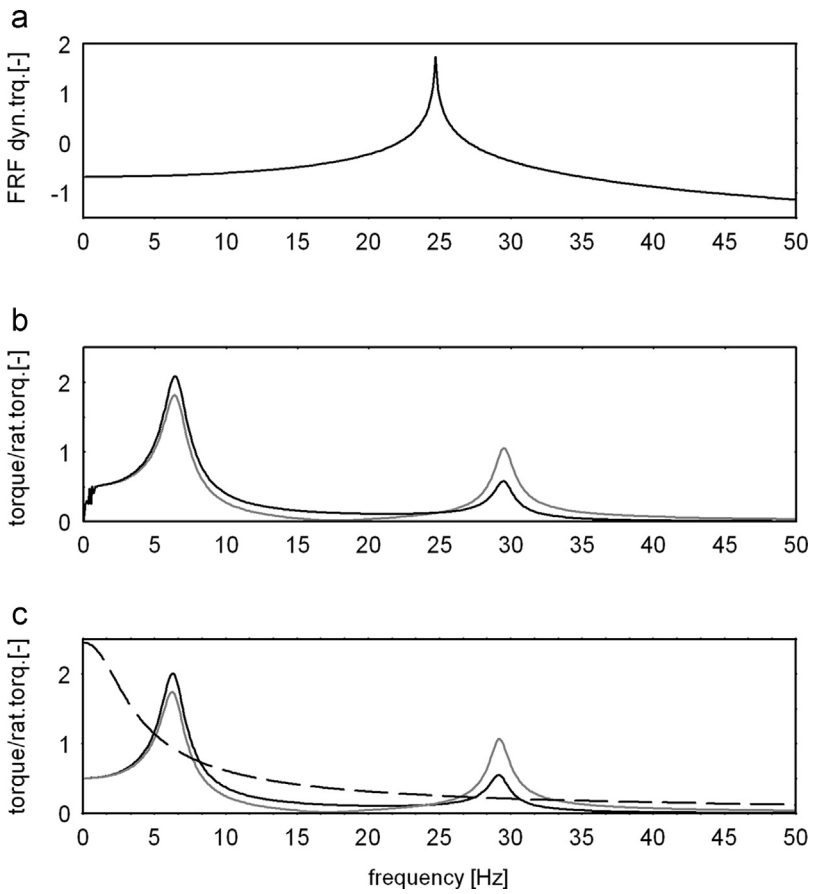

Fig. 12. Calculated frequency response function of the mechanical system (a), amplitude characteristics of the electromagnetic torque (solid black and dashed line) and of the mechanical torque in the shaft (gray line) obtained using simulation (b) and by means of the analytical solution (c).

these characteristics are depicted in Fig. 12b and c. This fact has been additionally confirmed by the results of simulation in time domain performed for the above mentioned resonant frequency 29.2 Hz. These results are presented in Fig. 13a and b in an identical way as those in Figs. 5 and 11. In Fig. 13a, the black and gray lines respectively demonstrate time histories of the electromagnetic motor torque and of the driven machine retarding torque. In Fig. 13b the mutually overlying time histories of dynamic torques transmitted by the input shaft connecting the motor with the rigid coupling (black line) and by the output shaft connecting the rigid coupling with the driven machine working tool (gray line) are depicted, see Fig. 13.

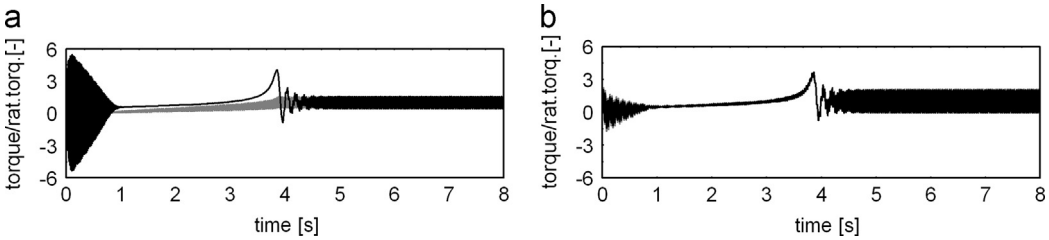

Fig. 13. Simulated resonant dynamic response of the centrifugal blower drive system.

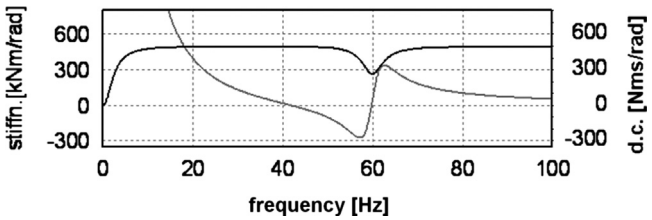

Fig. 14. Electromagnetic stiffness (black line) and damping coefficient (gray line).

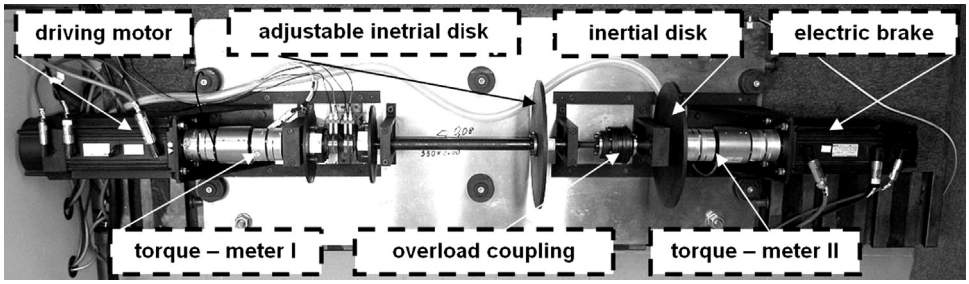

Fig. 15. Laboratory drive system of the rotating machine.

In the considered example the character of the dynamic interaction between the drive system and the asynchronous motor can be also explained by means of the motor electromagnetic stiffness and damping coefficient characteristics demonstrated in Fig. 14 in the same way as the analogous functions in Fig. 8. On the one hand, the shift of the fundamental torsional vibration 'elastic' resonant frequency from 24.7 to 29.2 Hz can be substantiated by the additional stiffening of the investigated torsional train by the driving motor electromagnetic flux. Here, this rotor-to-stator electromagnetic stiffness for interaction frequencies bigger than 15 Hz reaches 500 kNm/rad, where the first eigenmode torsional stiffness of the purely mechanical system $\omega_{1\gamma_1}^{2\,2}=1325.2$ kNm/rad is significantly greater, but still comparable to be remarkably influenced. On the other hand, as shown in Fig. 14, the electromagnetic damping coefficient in this interaction frequency range is already not high enough to completely attenuate the resonance effect. Similarly as in the previous example, the maximum dynamic response occurring at 6.4 Hz is also of a quasi-static character, since it does not indicate any dynamic amplification, too. These severe low-frequency torsional vibrations are either induced by the very high electric motor torque amplitudes occurring at low interaction frequencies, which follow from the motor-torque characteristic depicted by the dashed line in Fig. 12c and determined using Eqs. (9) and (10) for the constant rotor angular speed fluctuation amplitudes G and H arbitrarily assumed within the entire studied frequency domain. Moreover, the considered asynchronous motor is also characterized by a dangerous negative electromagnetic damping zone observed here in the range between 40 and 60 Hz, see Fig. 14.

Upon analyzing the results obtained in both considered examples one can ask a question, if all drive systems co-operating with the asynchronous motors indicate such a character of mutual dynamic interaction as that described above. The negative answer to this question is going to be substantiated in the following computational–experimental example.

5.3. *Example III: laboratory test-rig drive system*

The static torque characteristics of the asynchronous motors applied in both the previous examples and presented in Figs. 3 and 10a are characterized by very high driving torque gradients in the vicinity of nominal rotational speed value and by the relatively narrow rotational speed ranges of a stable operation. It is to remark that these features seem to be quite common for larger asynchronous motors. In this computational example for the laboratory drive system of a rotating machine presented in Fig. 15 the 2.1 kW asynchronous motor is used, where its static torque characteristic is characterized

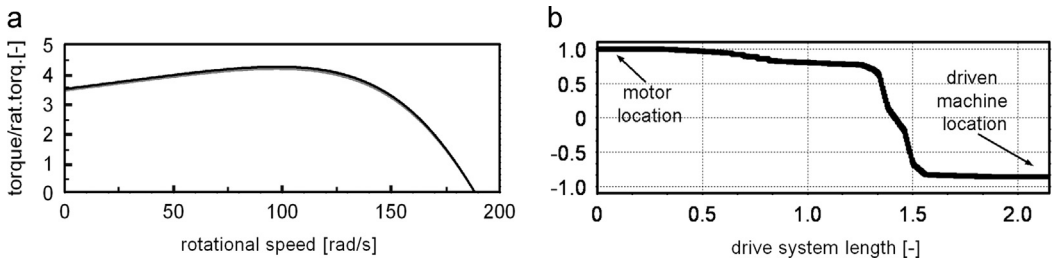

Fig. 16. Static torque characteristic of the driving motor (a) and the first eigenform of the drive system (b).

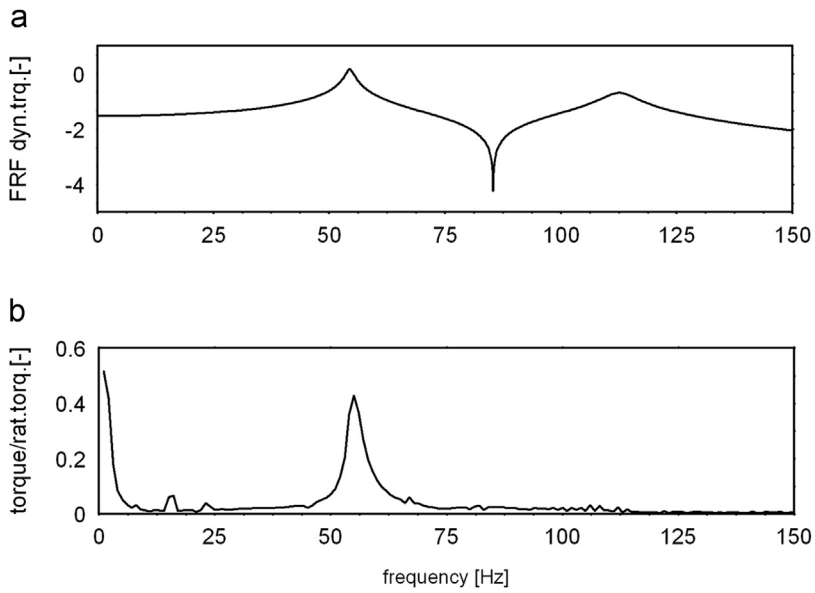

Fig. 17. Calculated frequency response function of the mechanical system (a) and amplitude characteristic of the measured dynamic torque registered by torque-meter I (b).

by the relatively small driving torque gradient in the neighborhood of nominal rotational speed and by the wider stable operation zone, as shown in Fig. 16a. The considered laboratory drive system is equipped with two torque-meters, i.e. "torque-meter I" installed between the driving motor and the adjustable inertial disk as well as "torque-meter II" situated between the overload coupling and the electric brake imitating an operation of the driven machine, see Fig. 15. By means of the frequency generator co-operating with the electric brake it was possible to impose the sinusoidal component on the average retarding torque transmitted by the entire drive system. These devices enabled us to determine experimentally the first two torsional 'elastic' natural frequencies equal to ~54.5 and ~112.1 Hz for the turned-off driving motor.

Then, similarly as in the first example described in Section 5.1, the hybrid model of the investigated laboratory drive system has been properly tuned-up in order to indicate the respective fundamental torsional natural frequencies possibly close to those obtained experimentally as well as to identify the mechanical damping level. The first torsional eigenform of natural frequency 54.6 Hz of this drive system model is presented in Fig. 16b. Fig. 17a illustrates the frequency response function of this model in the most important frequency range 0–150 Hz, in which the significant peaks corresponding to the above mentioned first two torsional natural frequencies are observed.

In the next step, the laboratory drive system was experimentally tested in nominal, steady-state operating conditions for the supply voltage frequency set-up to $\omega_e/2\pi=60$ Hz, where on the rated torque of the fluctuating sinusoidal component of amplitude $R=0.25$ of the constant value has been imposed by the electric brake within the practically most important excitation frequency range $\omega/2\pi=0$–150 Hz. In Fig. 17b the amplitude spectrum determined by means of FFT of the measured dynamic torque time histories registered using torque-meter I is presented. Apart from the visible disturbances introduced by the excitation signal at ca. 16 and 23 Hz, in this figure one can notice the significant peak corresponding to ca. 54.5 Hz, which is related to the resonance effect with the system first, fundamental 'elastic' natural frequency. Moreover, a dynamic amplification of the system response caused by the resonance effect with the second eigenform is also remarkable in the vicinity of 112 Hz.

Similarly as in the first example described in Section 5.1, in the retarding torque fluctuation frequency domain ω in Fig. 18a the plots of steady-state dynamic response fluctuation amplitudes are shown which are determined by successive

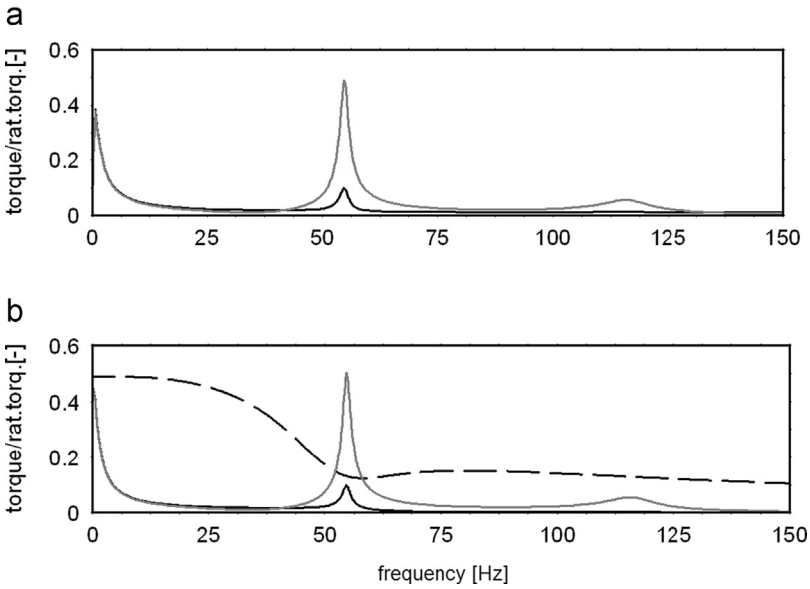

Fig. 18. Amplitude characteristics of the electromagnetic torque (solid black and dashed line) and of the mechanical torque in the input shaft (gray line) obtained using simulations (a) and by means of the analytical solution (b).

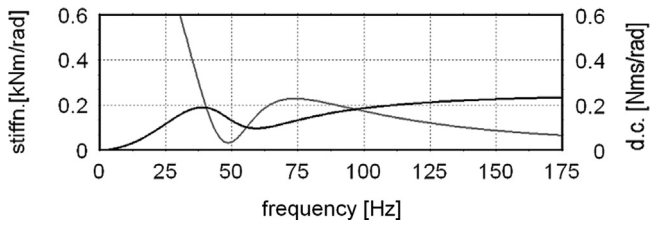

Fig. 19. Electromagnetic stiffness (black line) and damping coefficient (gray line).

numerical simulations performed for the analogous system nominal operating conditions as these realized during measurements, i.e. for the supply voltage frequency set-up to $\omega_e/2\pi=60$ Hz. In this figure the black and gray lines, respectively, there are plotted amplitudes of the motor-torque and of the dynamic torque transmitted by the input shaft in the vicinity of the torque-meter I position in the real object. The result depicted in Fig. 18a and determined by successively repeated simulations performed for each constant excitation frequency values $\omega/2\pi$ within 0–150 Hz has been very precisely confirmed by the analogous plots in Fig. 18b obtained using analytical relationships (10)–(12) and illustrated in the same way as those in Fig. 18a. As it follows from the electromechanical response amplitude characteristics: in Fig. 17b obtained experimentally and in Fig. 18a obtained using simulations as well as from that shown in Fig. 18b and determined by means of the analytical approach, apart from the quasi-static, low-frequency torsional oscillations excited due to the electromechanical interaction with the asynchronous motor within 0–4 Hz, all these amplitude characteristics are characterized by the resonant peaks at the above mentioned mechanical system natural frequencies $\sim$54.6 and $\sim$112.1 Hz, similarly as the frequency response function in Fig. 17a. In the considered case, this asynchronous motor is not able to influence remarkably the drive system dynamic properties, since in the entire investigated interaction frequency range 0–175 Hz the rotor-to-stator electromechanical stiffness does not exceed 0.25 kNm/rad, as shown in Fig. 19 which demonstrates the motor electromagnetic stiffness and damping coefficient characteristics. Here, the first eigenmode torsional stiffness of this mechanical system $\omega_1^2\cdot\gamma_1^2=12548.8$ kNm/rad is incomparably greater to be essentially influenced by any stiffening effect generated by this asynchronous motor. Moreover, the electromagnetic damping coefficient in the vicinity of 50 Hz is close to zero, but it is always positive within the entire considered interaction frequency range, as it follows from the respective plot in Fig. 19.

6. Final remarks

In the paper dynamic electromechanical coupling between the structural model of the rotating machine drive system and the circuit model of the asynchronous motor has been investigated. By means of the analytical–computational approach an interaction between the fundamental torsional eigenmodes and the driving electromagnetic torque was studied in order

to determine the frequency zones of greater sensitivity to amplification of torsional vibrations as well as the frequency zones of significant attenuating activity of the electromagnetic damping. For this purpose, for selected electromechanical systems an influence of electromagnetic and retarding torque fluctuation on torsional vibration amplitudes was investigated. As objects of considerations the rotating machine drive systems of mutually diverse structures and driven by the asynchronous motors of various power and technical parameters were applied. From the obtained results of computations and measurements it follows that the coupling effects between the mechanical and electrical parts become significant for drive systems characterized by very small fundamental torsional 'elastic' natural frequencies and driven by asynchronous motors with great static torque gradients in the nominal speed ranges. Then, the first, fundamental natural frequency values, which usually result in relatively small modal stiffness, can be remarkably increased since the eigenforms corresponding to them become sensitive to effective stiffening by the electromagnetic elasticity generated by the driving motor.

Because the asynchronous motors generate relatively high electromagnetic damping in the lowest torsional excitation frequency ranges, resonance effects with the fundamental eigenmodes of the driven mechanical system can be completely suppressed. On the other hand, an ability of induction of the greatest electromagnetic torque fluctuation amplitudes in the lowest excitation frequency ranges, indicated by the asynchronous motors, results in severe torsional vibrations which are quasi-static in character due to simultaneous activity of the above mentioned electromagnetic damping. Nevertheless, amplitudes of these oscillations can exceed many times the transmitted rated toque values, as it is followed from the performed measurements and theoretical computations. A physical cause of these low-frequency fluctuations can be also be described as rotational vibrations of the drive system rigid body mode, where the restoring moment is generated by the electromagnetic visco-elastic spring created by a driving motor between the rotor and the stator. A frequency of these oscillations is greater, when the stiffness of this spring is higher. According to the above, one can conclude that the electromechanical coupling between the asynchronous motor and the driven machine introduces an additional 'rigid body' vibration form, in addition to the naturally existing torsional 'elastic' vibrations of the drive system. A severity and character of all of them depend on individual dynamic properties of the mechanical system as well as on electrical parameters of the driving motor.

As described above and demonstrated by means of the proper characteristics, the considered asynchronous motors generate the greatest electromagnetic damping at the lowest external excitation frequencies. From comparisons with the experimentally identified mechanical damping coefficient values it follows that in the lowest frequency ranges the electromagnetic damping can dissipate torsional vibration energy more effectively than the mechanical one. Moreover, in cases of asynchronous motors with the above mentioned great static torque gradients in the nominal speed ranges negative electromagnetic damping is also observed. This property can lead to a dangerously instable motor co-operation with weakly damped mechanical systems. Minima of these negative damping coefficients usually occur for frequencies corresponding to the vicinities of the nominal supply voltage frequencies. For greater excitation frequencies the electromagnetic damping coefficients 'come back' to positive values and next they gradually begin to tend to zero. Then, torsional vibrations of the drive systems start to be more and more effectively attenuated by mechanical damping, effectiveness of which naturally increases with an oscillation frequency.

It is to emphasize that the theoretically investigated effects of the dynamic interaction between the asynchronous motors and the driven mechanical systems have been successfully confirmed by the results of measurements performed on the real object. Thus, the proposed analytical–computational approach for electromechanical coupling investigations, even at the presented stage, seems to be a convenient and very effective tool for producers of various machine drive systems, enabling them of making right choices of optimal asynchronous motors for driven objects. Nevertheless, in the next step of research in this field a more advanced electrical model of the asynchronous motor is going to be applied. Properties of this model will be referred to these of the analogous three-dimensional spatial model of the electromagnetic flux between the stator and the rotor.

Acknowledgment

These investigations have been supported by the Polish National Centre of Research and Development of the Ministry of Science and Higher Education: Research Project PBR-N R03 0012 04.

References

[1] B.F. Evans, A.J. Smalley, H.R. Simmons, Startup of synchronous motor drive trains: the application of transient torsional analysis of cumulative fatigue assessment, ASME Paper, 85-DET-122, 1985.
[2] A. Laschet, Simulation von Antriebssystemen, Springer-Verlag, Berlin, Heidelberg, London, New-York, Paris, Tokio, 1988.
[3] P. Schwibinger, R. Nordmann, Improvement of a reduced torsional model by means of parameter identification, Trans. ASME, J. Vib., Acoust., Stress Reliab. Des. 111 (1989) 17–26.
[4] L. Harnefors, Analysis of subsynchronous torsional interaction with power electronic converters, IEEE Trans. Power Syst. 22 (1) (2007) 305–313.
[5] C. Concordia, Induction motor damping and synchronizing torques, AIEE Trans. Power Appar. Syst. 71 (1952) 364–366.
[6] H. Berger, T.S. Kulig, Simulation models for calculating the torsional vibrations of large turbine-generator units after electrical system faults, Siemens Forsch. — u. Entwickl. Ber. 10 (4) (1981) 237–245.
[7] T. Iwatsubo, Y. Yamamoto, R. Kawai, Start-up torsional vibration of rotating machine driven by synchronous motor, in: Proceedings of the International Conference on Rotordynamics, IFToMM, Tokyo, Japan, 1986, pp. 319–324.

[8] A. Tabesh, R. Iravani, On the application of the complex torque coefficients method to the analysis of torsional dynamics, IEEE Trans. Energy Convers. 20 (2) (2005) 268–275.
[9] K. Xu, C. Zhao, J. Zhang, C. Guo, The application of complex torque coefficient method in multi-generator system, in: X. Wan (Ed.), Electrical Power Systems and Computers, LNEE 99, Springer-Verlag, Berlin Heidelberg, 2011, pp. 299–306.
[10] A.-K. Repo, P. Rasilo, A. Arkkio, Dynamic electromagnetic torque model and parameter estimation for a deep-bar induction machine, Electr. Power Appl., IET 2 (3) (2008) 183–192.
[11] T.P. Holopainen, A.-K. Repo, J. Järvinen, Electromechanical interaction in torsional vibrations of drive train systems including an electrical machine, in: Proceedings of the 8th IFToMM International Conference on Rotordynamics, KIST, Seoul, Korea, September 12–15, 2010, pp. 986–993.
[12] S. Del Puglia, S. De Franciscis, S. Van de Moortel, P. Jorg, T. Hattenbach, D. Sgrò, L. Antonelli, S. Falomi, Torsional interaction optimization in a LNG train with a load commutated inverter, in: Proceedings of the 8th IFToMM International Conference on Rotordynamics, KIST, Seoul, Korea, September 12–15, 2010, pp. 994–1001.
[13] K. Tanaka, H. Nemoto, N. Takahashi, Y. Fukushima, Y. Akita, M. Tobise, Measurement and simulation of forced torsional vibration with interharmonic frequencies in variable speed drive motor driven compressor, in: Proceedings of the 8th IFToMM International Conference on Rotordynamics, KIST, Seoul, Korea, September 12–15, 2010, pp. 844–851.
[14] T. Szolc, A. Pochanke, Dynamic investigations of electromechanical coupling effects in the mechanism driven by the stepping motor, J. Theor. Appl. Mech. 50 (2) (2012) 653–673.
[15] T. Szolc, On the discrete-continuous modeling of rotor systems for the analysis of coupled lateral–torsional vibrations, Int. J. Rotating Mach. 6 (2) (2000) 135–149.
[16] T. Szolc, P. Tauzowski, R. Stocki, J. Knabel, Damage identification in vibrating rotor-shaft systems by efficient sampling approach, Mech. Syst. Signal Process. 23 (2009) 1615–1633.
[17] K.L. Shi, T.F. Chan, Y.K. Wong, L.S. Ho, Modeling and simulation of the three-phase induction motor using SIMULINK, Int. J. Electr. Eng. Educ. 36 (1999) 163–172.